ZnO-CoS heterostructure quantum dots for enhanced electrocatalytic nitrogen reduction to ammonia

Yuyao Ji,[a]* Qiang Hu,[b] Mingyu Yang,[c] and Xingquan Liu [a,b]*

[a]College of Chemistry and Materials Science, Sichuan Normal University, Chengdu 610068, China. E-mail: yyji@sicnu.edu.cn

[b]School of Materials and Energy, University of Electronic Science and Technology of China, Chengdu 610054, China. lxquan@uestc.edu.cn

[c] College of Physics and Engineering, Chengdu Normal University, Chengdu. 611130, Sichuan, China.

Content:

Experimental section

Materials: Zinc nitrate hexahydrate ($Zn(NO_3)_2 \cdot 6H_2O$), ammonium fluoride (NH4F), urea (CH_4N_2O), cobalt nitrate hexahydrate ($Co(NO_3)_2 \cdot 6H_2O$), thiourea (CH_4N_2S), hydrochloric acid (HCl), and ethanol (C_2H_5OH) were purchased from Aladdin Reagent Inc. Nickel foam was purchased from Shenzhen Neware Electronics Co. Ltd. The ultrapure water used in the whole experiments was purified by a Millipore system. All related chemicals in the experiments can be used without further purification.

Preparation of ZnO-CoS QD: A certain amount of $Zn(NO_3)_2 \cdot 6H_2O$, $Co(NO_3)_2 \cdot 6H_2O$, CH_4N_2S and glucose with a weight ratio of 4:3:1:1 was dissolved in 25 mL of H_2O then sonicated for 30 min. Then the solution was transferred to a 50 mL Teflon-lined stainless-steel autoclave and heated in an oven at 180 °C for 12 h. The product was collected by centrifugation at 10000 rpm for 10 min, followed by repeatedly washing with water and finally drying by freeze-drying. Afterward, the samples were carbonized at 750 °C under argon atmosphere for 4 h with a heating rate of 5 °C min^{-1} to get the final products.

Preparation of ZnO-CoS QD electrode: 10 mg ZnO-CoS powders and 40 μL of Nafion solution (5 wt%) were dispersed in 960 μL mixed solution containing 720 μL ethanol and 240 μL H_2O by 2 h sonication to form a homogeneous ink. Then, 10 μL ZnO-CoS QD was loaded on a CP with area of 1 x 1 cm^2 and dried under ambient condition.

Characterizations: XRD patterns were obtained from a Shimazu XRD-6100 diffractometer with Cu Kα radiation (40 kV, 30 mA) of wavelength 0.154 nm (Japan). SEM images were collected from the tungsten lamp-equipped SU3500 scanning electron microscope at an accelerating voltage of 20 kV (HITACHI, Japan). TEM images were obtained from a Zeiss Libra 200FE transmission electron microscope operated at 200 kV. XPS measurements were performed on an ESCALABMK II X-ray photoelectron spectrometer using Mg as the exciting source. The UV-Vis absorbance spectra were measured on a SHIMADZU UV-1800 UV-Vis spectrophotometer. energy dispersive X-ray analysis (EDX), and the Brunner−Emmet−Teller method (BET, ASAP 2020, Micromeritics).

Electrochemical measurements: Before NRR measures, the Nafion proton exchange film was pretreated by heating in 3% H_2O_2 solution, 0.5 M H_2SO_4 and ultrapure water at 80 °C for

1.5 h, respectively. Electrochemical measurements were carried out on a CHI 660E electrochemical analyzer (CHI Instruments, Inc., Shanghai) in a three-electrode system using ZnO-CoS QD or CP as working electrode, Ag/AgCl as reference electrode, and graphite rod as counter electrode. All experiments were performed at ambient conditions. For N_2 reduction reaction experiments, the HCl electrolyte (0.1 M) was bubbled with high-purity N_2 (99.999%) for 30 min before measurement. All potentials reported in this work were calibrated to RHE, using the following equation:

$$E \text{ (RHE)} = E \text{ (Ag/AgCl)} + (0.197 + 0.059 \text{ pH}) \text{ V}$$

Determination of NH$_3$: NH_3 concentration was determined by the indophenol blue method.[1] The method contains the following details: 2 mL HCl post-NRR electrolyte was collected from the cathodic chamber. Then, 2 mL of 1 M NaOH solution containing 5% salicylic acid and 5% sodium citrate was added into this solution. After mixing and standing at room temperature for 2 h, the UV-Vis absorption absorption spectrum was measured at a wavelength of 655 nm. The concentration-absorbance curves were calibrated using standard NH_4Cl solution (0.1 HCl solution as mother solution) with a serious of concentrations. The fitting curve ($y = 0.475x + 0.066$, $R^2 = 0.999$) shows good linear relation of absorbance value with NH_3 concentration by three times independent calibrations.

Determination of N$_2$H$_4$: Concentration of N_2H_4 in the electrolyte was estimated by the method of Watt and Chrisp.[2] Typically, a mixture solution containing p-$C_9H_{11}NO$ (5.99 g), concentrated HCl (30 mL) and ethanol (300 mL) was used as a color reagent. In detail, 2 mL electrolyte removed from the cathodic chamber was added into 2 mL above prepared color reagent. After standing the mixture solution at room temperature for 20 min, UV-Vis absorption spectra were measured at a wavelength of 455 nm. The concentration-absorbance curves were calibrated using standard N_2H_4 solutions with a series of concentrations for three independent calibrations.

Calculations of NH$_3$ yield and FE: NH_3 yield was calculated using the following equations:

$$R_{NH3} \text{ (µg h}^{-1} \text{ mg}_{cat.}^{-1}\text{)} = (c_{NH3} \times V) / (17 \times t \times m)$$

Where c_{NH_3} (μg mL^{-1}) is the measured NH$_3$ concentration; V (mL) is the volume of electrolyte (in our work 35 mL); t (s or h) is the reaction time; A (cm^2) is the geometric area of the cathode; m (mg) is the mass loading of catalyst on CP.

FE was calculated according to following equation:

$$FE = 3 \times F \times c_{NH_3} \times V / (17 \times Q) \times 100\%$$

Where F is Faraday constant (96500 C mol^{-1}); Q (C) is the quantity of applied electricity.

Computational details: To gain more in-depth insights into the mechanism for nitrogen reduction reaction (NRR) on ZnO-CoS, density functional theory (DFT) calculations are carried out using the Vienna ab initio simulation package (VASP). Exchange-correlation energy is described by Perdue-Burke-Ernzerhof (PBE) version of the generalized gradient approximation (GGA). The projector-augmented wave (PAW) method is used to represent the core-valence electron interaction. The calculations also adopt long-range dispersion interactions (DFT-D3 (BJ)) A Hubbard U term is introduced to the PBE functional, with U$_{eff}$ = 4.2 eV for Zn on its d orbital. An energy cutoff of 480 eV for basis-set expansion is used. A 2 × 2 supercell and the corresponding 5 × 5 × 1 k-point mesh are modeled in the calculations. A vacuum region of about 20 Å is set to decouple the periodic replicas. The groups attached to the hollow sites between the three neighboring carbon atoms are added on each side of CoS monolayer according to previous literatures. A OH group is removed to expose active sites for N$_2$ adsorption. The force tolerance and total energy for the relaxations are converged to 0.02 eV Å^{-1} and 10^{-5} eV, respectively. The Gibbs free energy is calculated via the computational hydrogen electrode model proposed by Nørskov et al.

$$\Delta G = \Delta E + \Delta ZPE - T\Delta S$$

T and pH value are set to be 298.15K and 0 in this work, respectively. For adsorbates, ZPE and S are determined by vibrational frequencies calculations. For molecules, those are taken from the NIST database.
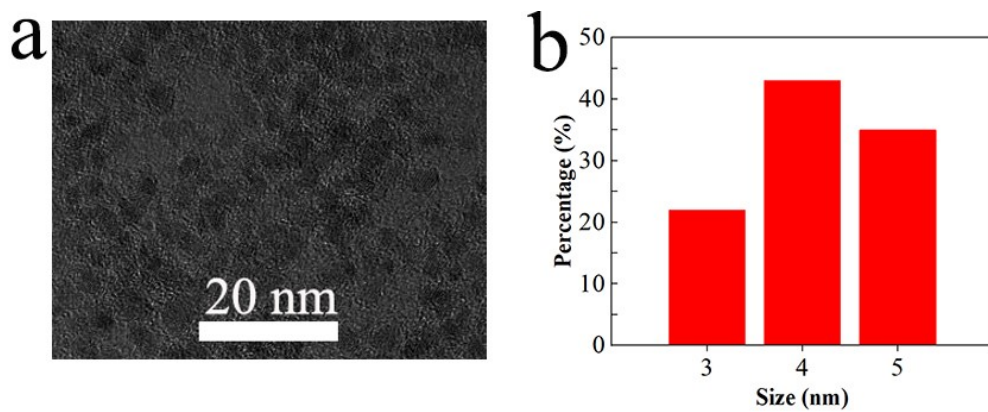
Fig. S1. (a) TEM image of ZnO-CoS QD. (b) corresponding dot size distribution histogram of the ZnO-CoS QD.
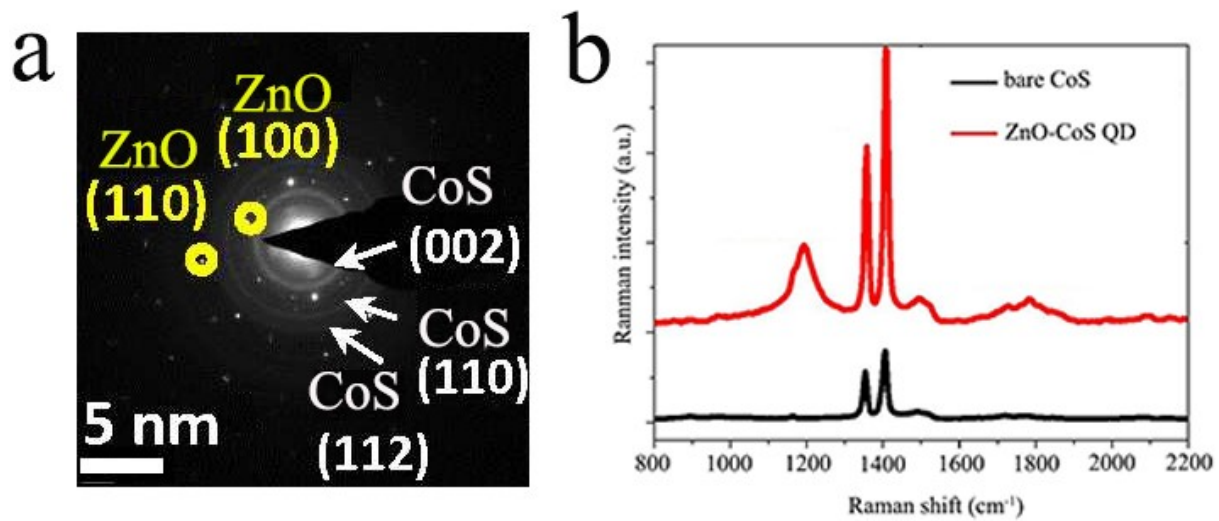
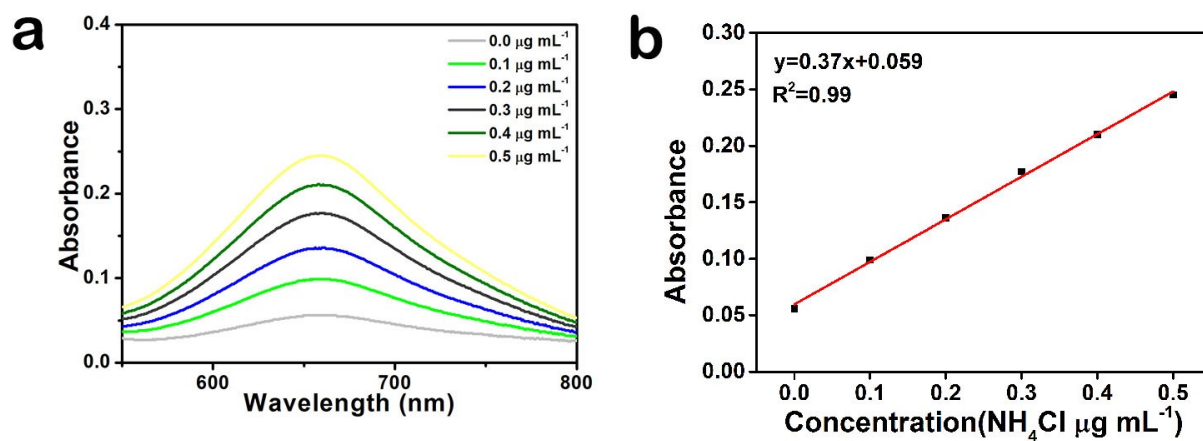**Fig. S2.** (a) SAED patterns of ZnO-CoS QD. (b) Raman spectra for CoS and ZnO-CoS QD Heterostructures.

Fig. S3. (a) UV-Vis absorption spectra of indophenol assays with NH^{4+} concentrations after incubated for 2 h at room temperature. (b) Calibration curve used for calculation of NH^{4+} concentrations.
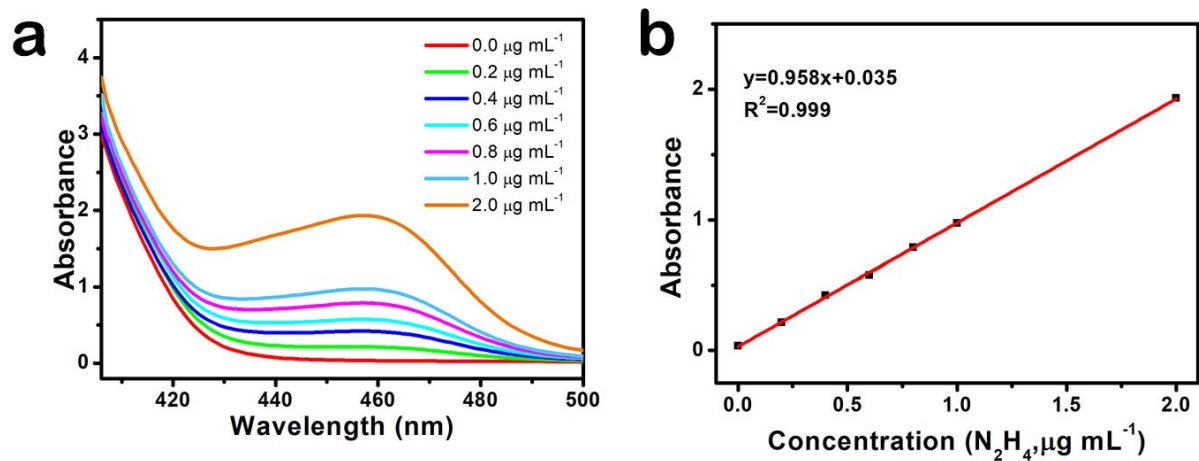
Fig. S4. (a) UV-Vis absorption spectra of various N_2H_4 concentrations after incubated for 15 min at room temperature. (b) Calibration curve used for calculation of N_2H_4 concentrations.
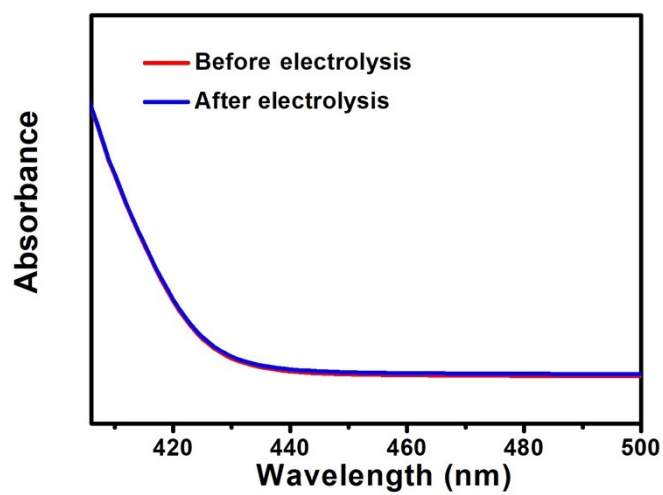
Fig. S5. UV-Vis absorption spectra of the electrolytes estimated by the method of Watt and Chrisp before and after 2 h electrolysis in N_2 atmosphere at –0.2 V.
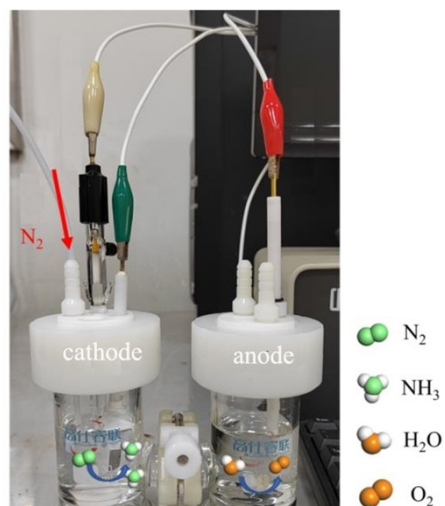
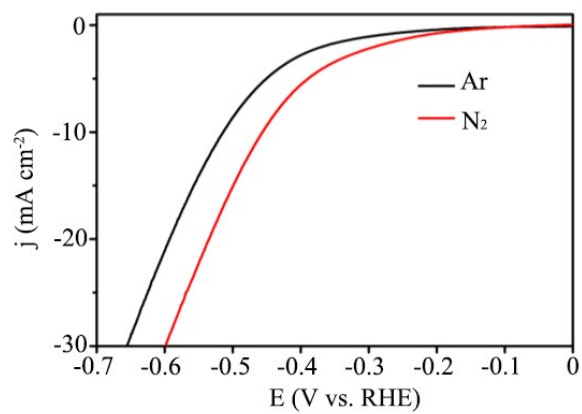**Fig. S6.** The photograph of electrochemical setup for NRR test.

Fig. S7. LSV curves of ZnO-CoS QD in Ar- and N_2- saturated solutions.
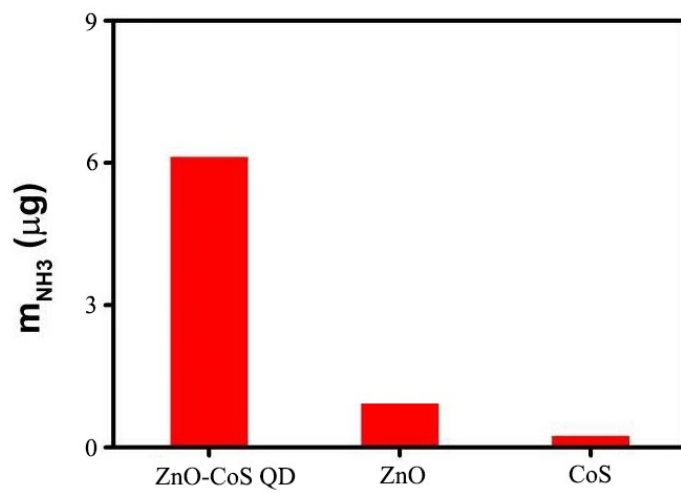
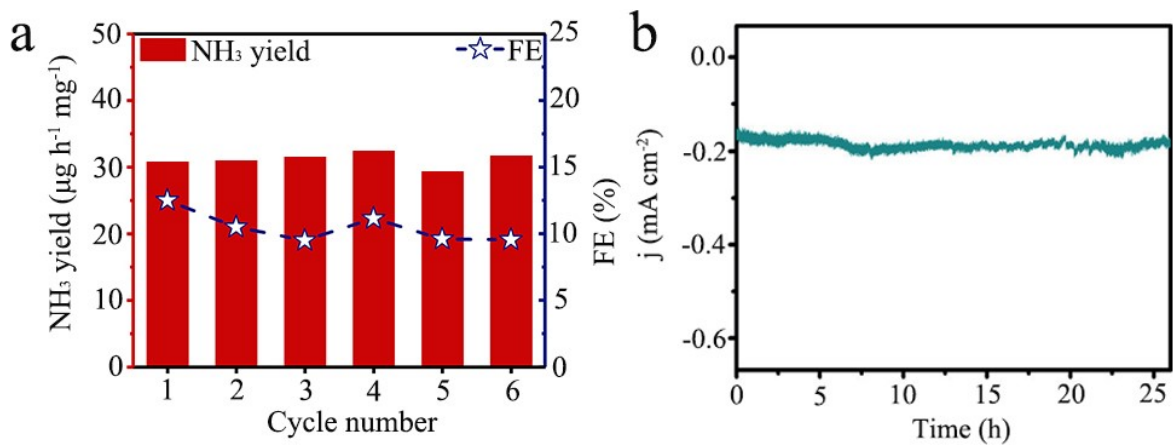**Fig. S8.** Amount of NH_3 produced for ZnO-CoS QD, ZnO and CoS.

Fig. S9. (a) NH$_3$ yield rate and FE of cycling tests at -0.2 V. (b) Time-dependent current density curve of ZnO-CoS QD at -0.2 V for 26 h.
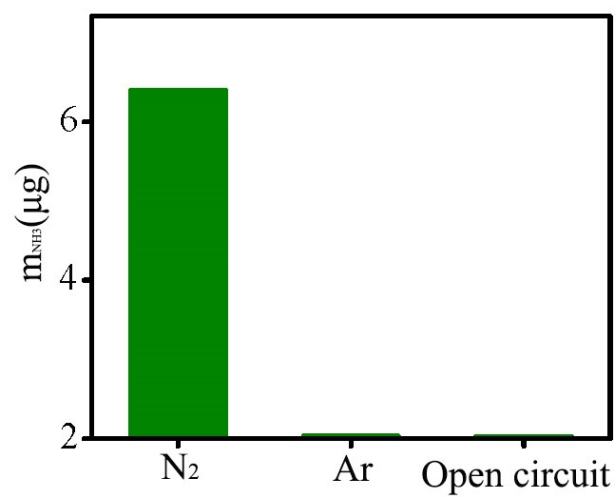
Fig. S10. The amount of NH$_3$ produced for ZnO-CoS QD under different electrochemical conditions.
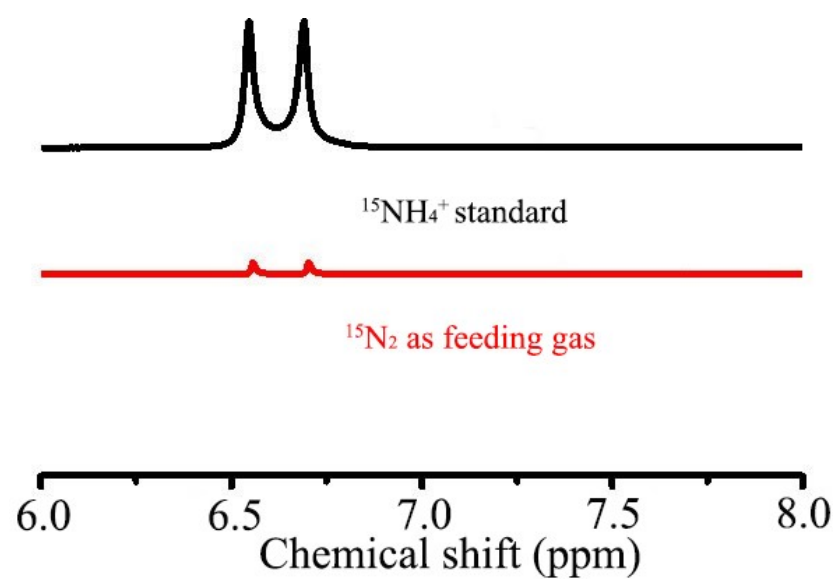
Fig. S11. ^{15}N isotope labeling experiment. ^{1}H NMR spectra for the post electrolysis 0.1 M Na$_2$SO$_4$ electrolytes with ^{15}N$_2$ as feeding gas.

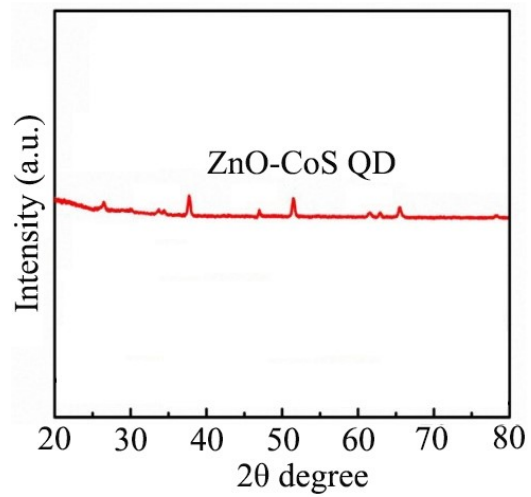**Fig. S12.** XRD patterns of Zn-CoS QD after stability testing.
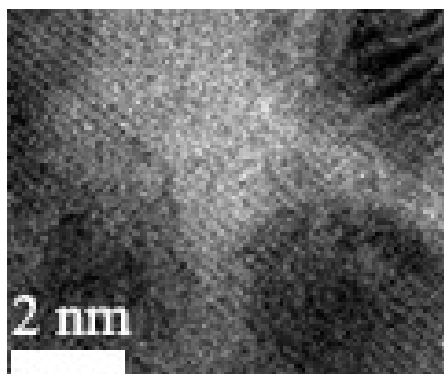
Fig. S13. TEM image of Zn-CoS QD after stability testing.

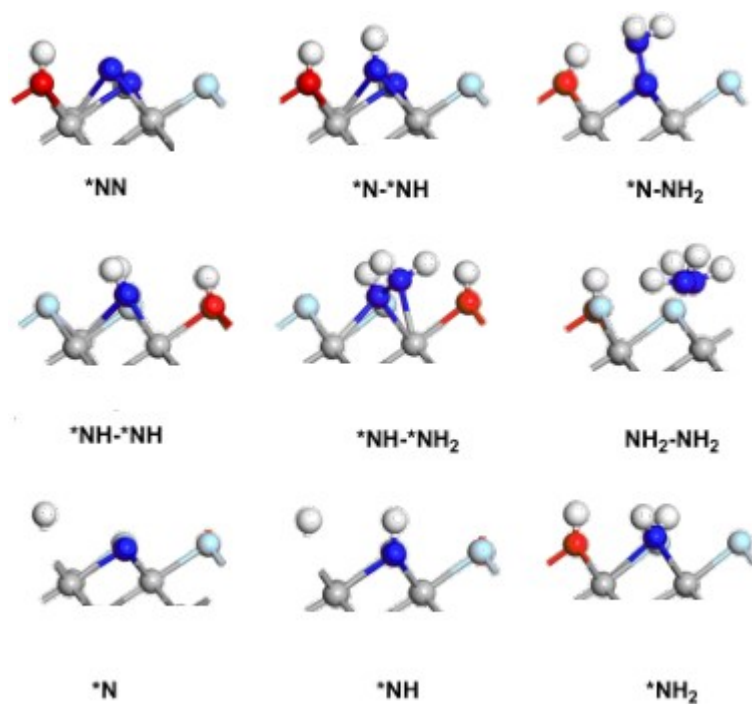**Fig. S14.** Optimized geometric structures of intermediates along the reaction path. Colour code: light grey, Zn; dark grey, O; blue, Co; red, S; white, H.
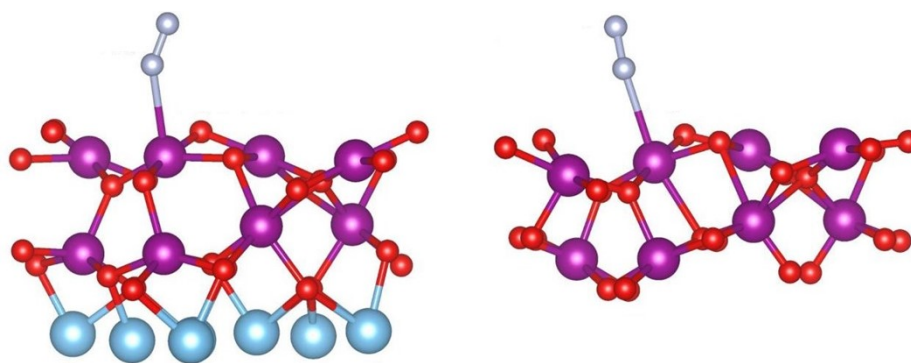
Fig. S15. Gibbs energy profile for the N_2 reduction process, performed on ZnO-CoS surface, through traditional distal pathway.
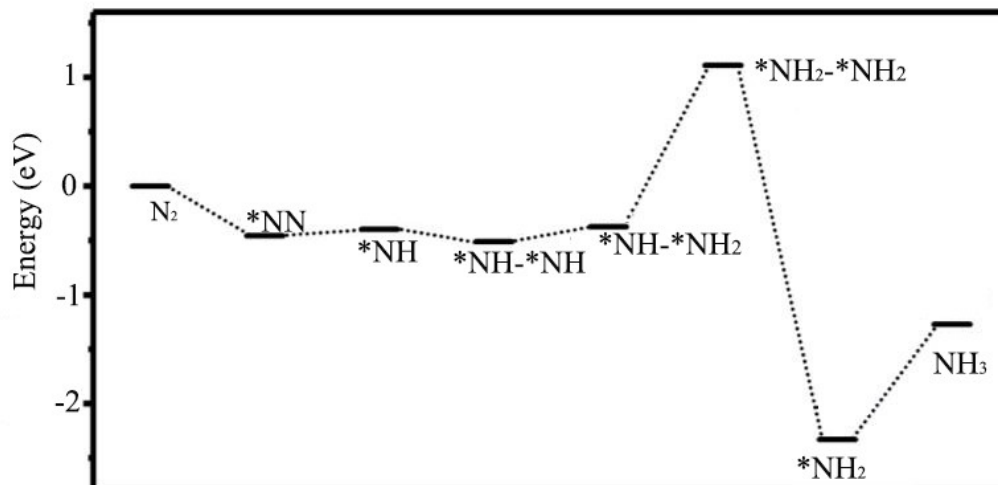
Fig. S16. DFT calculated energy profile for the electrocatalytic N_2 reduction reaction on the ZnO.

Table S1. Comparison of electrocatalytic N_2 reduction performance for ZnO-CoS QD with other electrocatalysts under ambient conditions.

Catalyst	Electrolyte	NH$_3$ yield rate (μg h^{-1} mg$_{cat.}^{-1}$)	FE (%)	Ref.
ZnO-CoS QD	**0.1 M Na$_2$SO$_4$**	**33.03**	**11.7**	**This work**
ZnO QD	-	17.7	6.4	4
PdPb/C	0.1 M HCl	25.68	5.79	5
Pd-Ag-S	0.1 M Na$_2$SO$_4$	9.73	18.41	6
PdH$_{0.43}$NRs	0.1 M Na$_2$SO$_4$	17.53	18.56	7
DG-800	0.1 M Na$_2$SO$_4$	4.31	8.51	8
nPd/NF	0.1 M Na$_2$SO$_4$	18.27	10.36	9
etched-PdZn/NHCP	0.1 M PBS	5.28	16.9	10
Li-TiO$_2$	0.5 M LiClO$_4$	8.7	18.2	11
TiO$_2$-C	0.1 M Na$_2$SO$_4$	14.0	13.3	12
Mn-TiO$_2$	0.1 M Na$_2$SO$_4$	20.05	11.93	13
P-TiO$_2$	0.5 M LiClO$_4$	25.05	12.26	14
Fe$_1$S$_x$-TiO$_2$	0.1 M HCl	18.3	17.3	15
La-TiO$_2$	0.1 M LiClO$_4$	23.06	14.54	16
Fe-doped SnO$_2$	0.1 M Na$_2$SO$_4$	28.45	6.54	17

References

1   D. Zhu, L. Zhang, R. E. Ruther and R. J. Hamers, Photo-illuminated diamond as a solid-state source of solvated electrons in water for nitrogen reduction. *Nat. Mater.*, 2013, **12**, 836–841.

2   G. W. Watt and J. D. Chrisp, Spectrophotometric method for determination of hydrazine. *Anal. Chem.*, 1952, **24**, 2006–2008.

3   G. Kresse and J. Furthmüller, Efficient iterative schemes for Ab initio total-energy calculations using a plane-wave basis set. *Phys. Rev. B.*, 1996, **54**, 11169.

4   Y. Liu, Y. Li, D. Huang, H. Zhang and K. Chu, ZnO Quantum dots coupled with graphene toward electrocatalytic N_2 reduction: Experimental and DFT Investigations. *Chem. Eur. J.*, 2019, **25**, 11933–11939

5   H. Zhao, D. Zhang, Z. Wang, Y. Han, X. Sun, H. Li, X. Wu, Y. Pan, Y. Qin and S. Lin, High-performance nitrogen electroreduction at low overpotential by introducing Pb to Pd nanosponges. *Appl. Catal. B*, 2020, **265**, 118481.

6   H. Wang, S. Liu, H. Zhang, S. Yin, Y. Xu, X. Li, Z. Wang and L. Wang, Three-dimensional Pd-Ag-S porous nanosponges for electrocatalytic nitrogen reduction to ammonia. *Nanoscale*, 2020, **12**, 13507-13512.

7   Z. Wang, Z. Dai, S. Wang, H. Zhang, W. Tian, Y. Xu, X. Li, L. Wang and H. Wang, Enhancing electrochemical ammonia synthesis on palladium nanorods through surface hydrogenation. *Chem. Eng. J.*, 2021, **416**, 129105.

8   Y. Du, C. Jiang, W. Xia, L. Song, P. Li, B. Gao, C. Wu, L. Sheng, J. Ye, T. Wang and J. He, Electrocatalytic reduction of N_2 and nitrogen-incorporation process on dopant-free defect graphene. *J. Mater. Chem. A*, 2020, **8**, 55-61.

9   Z. Wang, Z. Dai, H. Yu, H. Zhang, W. Tian, Y. Xu, X. Li, L. Wang and H. Wang, Antioil Ag_3PO_4 nanoparticle/polydopamine/Al_2O_3 sandwich structure for complex wastewater treatment: dynamic catalysis under natural light. *ACS Sustain. Chem. Eng.*, 2020, **8**, 11827–11833.

10   M. Ma, X. Han, H. Li, X. Zhang, Z. Zheng, L. Zhou, J. Zheng, Z. Xie, Q. Kuang and L. Zheng, Tuning electronic structure of PdZn nanocatalyst via acid-etching strategy for

highly selective and stable electrolytic nitrogen fixation under ambient conditions. *Appl. Catal. B*, 2020, **265**, 118568.

11   R. Zhao, G. Wang and Y. Mao, Li-Intercalation boosted oxygen vacancies enable efficient electrochemical nitrogen reduction on ultrathin TiO_2 nanosheets, *Chem. Eng. J.*, 2022, **430**, 133085.

12   G. Zhao, X. Wang and C. Xu, MXene-derived nanocomposites as earth-abundant efficient electrocatalyst for nitrogen reduction reaction under ambient conditions, *Inorg. Chem.*, 2020, **59**, 16672-16678.

13   H. Chen, T. Wu, X. Li, S. Lu, F. Zhang, Y. Wang, H. Zhao, Q. Liu, Y. Luo, A.M. Asiri, Z. Feng, S Zhang and X. Sun, Modulating oxygen vacancies of TiO_2 nanospheres by Mn-doping to boost electrocatalytic N_2 reduction, *ACS Sustain. Chem. Eng.*, 2021, **9**, 1512-1517

14   P. Zhao, L. Zhang, J. Song, S. Wen and Z. Cheng, Phosphorus cation substitution in TiO_2 nanorods toward enhanced N_2 electroreduction, *App. Sur. Sci.*, 2020, **523**, 146517.

15   J. Chen, Y. Kang, W. Zhang, Z. Zhang, Y. Chen, Y. Yang, L. Duan, Y. Li and W. Li, Lattice-confined single-atom Fe_1S_x on mesoporous TiO_2 for boosting ambient electrocatalytic N_2 reduction reaction, *Angew. Chemie Int. Edit.*, 2022, **61**, e202203022.

16   L. Li, H. Chen, L. Li, B. Li, Q. Wu, C. Cui, B. Deng, Y. Luo, Q. Liu, T. Li, F. Zhang, A.M. Asiri, Z. Feng, Y. Wang and X. Sun, La-doped TiO_2 nanorods toward boosted electrocatalytic N_2-to-NH_3 conversion at ambient conditions, *Chin. J. Catal.*, 2021, **42**, 1755-1762.

17   Y. Li, Y. Liu, X. Liu, Y. Liu, Y. Cheng, P. Zhang, P. Deng, J. Deng, Z. Kang and H. Li, Fe-doped SnO_2 nanosheet for ambient electrocatalytic nitrogen reduction reaction, *Nano Res.*, 2022, **15**, 6026-6035.